Structure and Physical Properties of $La_{3.4}Ca_{0.6}V_5Si_4O_{22}$: A Novel Mixed-Valent Vanadium(III/IV) Oxosilicate

S. C. Chen, K. V. Ramanujachary, and M. Greenblatt*

Department of Chemistry, Rutgers, The State University of New Jersey, Piscataway, New Jersey 08855-0939

Received June 23, 1994[⊗]

$La_{3.4}Ca_{0.6}V_5Si_4O_{22}$ crystallizes in the monoclinic system, space group $C2/m$ (No. 12). The unit cell dimensions are $a = 13.448(4)$ Å, $b = 5.5879(9)$ Å, $c = 11.070(4)$ Å, $\beta = 100.57(2)°$, $V = 817.7(4)$ Å^3, and $Z = 2$. Structural refinement with 817 observed reflections ($I > 3\sigma(I)$) and 103 variable parameters resulted in $R = 0.034$, $R_w = 0.037$. The structure of $La_{3.4}Ca_{0.6}V_5Si_4O_{22}$ may be described as the intergrowth of vanadium pyrosilicate layers, $V^{III}(Si_2O_7)_2^{9-}$, and rutile-like layers, $(VO_2)_4^{2.4-}$. These two layers are interconnected by corner-sharing oxygen atoms between Si_2O_7 groups and VO_6 octahedra in the rutile layers along the c-axis. Distorted octagonal tunnels running along the b-axis are created by the network of polyhedra. The La^{3+} and Ca^{2+} ions located in these tunnels are statistically disordered. The magnetic susceptibility of $La_{3.4}Ca_{0.6}V_5Si_4O_{22}$ follows a Curie−Weiss behavior with an effective moment indicative of two localized unpaired electrons in the $V^{III}(Si_2O_7)_2^{9-}$ layer. The $(VO_2)_4^{2.4-}$ rutile layer forms an extended V−V bond along the b-axis; however, $La_{3.4}Ca_{0.6}V_5Si_4O_{22}$ is an insulator with room-temperature resistivity of the order of 10^6 Ω cm along the b-axis.

Introduction

The synthesis and properties of reduced oxides whose structures contain a mixed framework built up from MO_6 (M = transition metal ion) octahedra and XO_4 (X = P or Si) tetrahedra have received considerable attention in recent years mostly due to their anisotropic transport properties that are a result of the association of metallic layers (or rows) of MO_6 interleaved with insulating rows (or layers) of XO_4. For example, the recently discovered phosphate−tungsten bronzes were shown to display interesting low-dimensional electronic properties including charge density wave driven structural phase transitions.[1] The existing literature on the reduced A−M−P−O (A = IA, IIA, or rare earth ion) has been comprehensively discussed in several review articles.[1,2] Although tetrahedral geometry is commonly observed for both the PO_4 and SiO_4 units, it is somewhat striking to note that only a few reduced transition metal silicates are known so far. To the best of our knowledge, $(Ba_3Nb_6Si_4O_{26})_n(Ba_3Nb_8O_{21})$ with $n = 1$[3] and $Ba_3Ta_6Si_4O_{23}$[4] are the only known reduced Nb or Ta oxosilicates. The prefix oxo here implies the presence of chains or layers of transition metal oxide networks that are isolated by silicate groups.[3a]

A large number of reduced vanadium phosphates and oxophosphates have been known for some time;[5-7] however, examples of reduced vanadium oxides containing silicate groups are rare. Reduced vanadium pyrosilicates such as $BaVSi_2O_7$ (α- and β-forms),[8] $SrVSi_2O_7$,[9] $Ba_2VSi_2O_8$,[10] and $Ca(VO)(Si_4O_{10}) \cdot 4H_2O$,[11] with square pyramidal $V(IV)O_5^{6-}$ units isolated by the $Si_2O_7^{6-}$ pyrosilicate groups have been reported. Reduced vanadium silicates with extended V−V or V−O−V interactions, however, are not known yet. Furthermore, mixed-valent vanadium, although is known in phosphates,[7] has not been observed in silicate compounds so far. In this paper, the single-crystal structure and physical properties of the first mixed-valent vanadium oxosilicate, $La_{3.4}Ca_{0.6}V_5Si_4O_{22}$, are reported.

Experimental Section

Materials. Prior to use, La_2O_3 (Aldrich, 99.9+%) was heated at 1100 °C for 12 h and V_2O_5 (Aldrich, 99.99%) at 500 °C for 6 h in air. CaO (Aldrich, 99.9%), $CaCl_2$ (Strem Chemicals, 99.99%), and V (Aldrich, 99.5%, 325 mesh) were used as obtained without further purification.

Synthesis. In an attempt to grow single crystals of $La_2CaV_2O_7$ in $CaCl_2$ flux, a reaction mixture containing La_2O_3, CaO, V_2O_5, and V in a molar ratio of 1 : 1 : 0.6 : 0.8 (aimed at $La_2CaV_2O_7$) was weighed out and thoroughly mixed with $CaCl_2$ (5% by weight), and the mixture was pelletized by hand-pressing a dye in a He-filled drybox. The loosely pressed pellet was later sealed in a double-jacket quartz tube and then heated at 1250 °C for 6 days. Black needle crystals of $La_{3.4}Ca_{0.6}V_5Si_4O_{22}$ and platelike crystals of V_2O_3 were recovered after washing the product with water.

* To whom correspondence should be addressed.

⊗ Abstract published in *Advance ACS Abstracts,* November 15, 1994.

(1) Greenblatt, M. *Int. J. Mod. Phys.* **1993**, *B7*, 3937.
(2) (a) Borel, M. M.; Goreaud, M.; Grandin, A.; Labbe, Ph.; Leclaire, A.; Raveau, B. *Eur. J. Solid State Inorg. Chem.* **1991**, *28*, 93. (b) Raveau, B.; Borel, M. M.; Leclaire, A.; Grandin, A. *Int. J. Mod. Phys.* **1993**, *B7*, 4109. (c) Benabbas, A.; Provost, J.; Borel, M. M.; Leclaire, A.; Raveau, B. *Chem. Mater.* **1993**, *5*, 1143. (d) Costentin, G.; Leclaire, A.; Borel, M. M.; Grandin, A.; Raveau, B. *Rev. Inorg. Chem.* 1993, *13*, 77. (e) Haushalter, R. C.; Mundi, L. A. *Chem. Mater.* **1992**, *4*, 31.
(3) (a) Serra, D. L.; Hwu, S.-J. *J. Solid State Chem.* **1992**, *101*, 32. (b) Evans, D. M.; Katz, L . *J. Solid State Chem.* **1973**, *8*, 150.
(4) Shannon, J.; Katz, L. *J. Solid State Chem.* **1970**, *1*, 399.
(5) (a) Benhamada, L.; Grandin, A.; Borel, M. M.; Leclaire, A.; Raveau, B. *ActaCrystallogr.* **1991**, *C47*, 2437. (b) Lii, K. H. *J. Chem. Soc., Dalton Trans.* **1994**, 931. (c) Lii, K. H.; Wang, Y. P.; Chen, Y. B.; Wang, S. L. *J. Solid State Chem.* **1990**, *86*, 143. (d) Lii, K. H.; Wen, N. S.; Su, C. C.; Chueh, B. R. *Inorg. Chem.* **1992**, *31*, 439. (e) Hwu, S.-J.; Willis, E. D. *J. Solid State Chem.* **1991**, *93*, 69.
(6) Haushalter, R. C.; Chen, Q.; Soghomonian, V.; Zubieta, J.; O'Connor, C. J. *J. Solid State Chem.*, **1994**, *108*, 128.
(7) (a) Leclaire, A.; Chardon, J.; Grandin, A.; Borel, M. M.; Raveau, B. *J. Solid State Chem.*, **1994**, *108*, 291. (b) Crespoa, P.; Grandin, A.; Borel, M. M.; Leclaire, A.; Raveau, B. *J. Solid State Chem.* **1993**, *105*, 307. (c) Kinomura, N.; Matsui, N.; Kumada, N.; Muto, F. *J. Solid State Chem.*, **1989**, *79*, 232. (d) Johnson, J. W.; Johnston, D. C.; King, H. E., Jr.; Halbert, T. R.; Brody, J. F.; Goshorn, P. *Inorg. Chem.* **1988**, *27*, 1646. (e) Lee, C. S.; Lii, K. H. *J. Solid State Chem.*, **1991**, *92*, 362.
(8) (a) Matsubara, S.; Kato, A.; Yui, S. *Mineral. J.* **1982**, *11*, 15. (b) Liu, G.; Greedan, J. E. *J. Solid State Chem.* **1994**, *108*, 267.
(9) Takeuchi, Y.; Joswig, W. *Mineral. J.* **1967**, *5*, 98.
(10) Feltz, V. A.; Schmalfuss, S.; Langbein, H.; Tietz, M. *Z. Anorg. Allg. Chem.* **1975**, *417*, 125.
(11) Evans, H. T., Jr. *Am. Mineral.* **1973**, *58*, 412.

0020-1669/94/1333-5994$04.50/0

Table 1. Selected X-ray Crystallographic Data for $La_{3.4}Ca_{0.6}V_5Si_4O_{22}$

empirical formula	$La_{3.4}Ca_{0.6}V_5Si_4O_{22}$	fw	1215.4
space group	$C2/m$ (No. 12)	T, °C	20
a, Å	13.448(4)	λ, Å	0.710 69
b, Å	5.5879(9)	d_{calcd}, g/cm^3	4.94
c, Å	11.070(4)	μ(Mo Kα), cm^{-1}	122.9
β, deg	100.57(2)	R^a	0.034
V, Å^3	817.7(4)	$R_w{}^b$	0.037
Z	2		

^{a} $R = \sum(|F_o| - |F_c|)/\sum|F_o|$. ^{b} $R_w = [\sum w(|F_o| - |F_c|)^2/\sum w|F_o|^2]^{1/2}$; $w = 1/(\sigma^2|F_o|)$.

A semiquantitative elemental analysis with a scanning electron microscope (AMRAY 1400) on a number of selected needle crystals (including the one used for the single-crystal X-ray crystallographic study) indicated the presence of La, Ca, V, and Si with an approximate molar ratio of 3 : 1 : 5 : 4. A more accurate composition was later established by the single-crystal X-ray structural refinement.

Single-Crystal X-ray Crystallographic Studies. A needle-shaped crystal with approximate dimensions of 0.36 × 0.02 × 0.01 mm^3 was selected for single-crystal X-ray crystallographic study. The preliminary lattice parameters were determined from oscillation and Weissenberg photographs. The final unit cell parameters were determined from a least-squares analysis of the setting angles of 25 carefully chosen reflections in the range 20° < 2θ < 30° automatically centered on an Enraf-Nonius CAD4 diffractometer. The intensity measurements were collected at room temperature. Graphite-monochromated Mo Kα radiation was employed to collect data in the range 4° ≤ 2θ ≤ 60°. An $\omega-\theta$ scan mode was used. Three standard reflections measured every 3 h showed no apparent decay in intensity during data collection. The intensity data were corrected for Lorentz–polarization effects. The linear absorption coefficient for Mo Kα is 122.9 cm^{-1}. An empirical absorption correction was applied, based on azimuthal scans of one reflection with transmission factors in the range from 0.826 to 0.996. A correction for secondary extinction was also applied in the structural refinement. In the quadrant ($\pm h,k,l$), 1301 unique reflections were collected, of which 817 reflections with $I > 3\sigma(I)$ were considered as observed and used in the subsequent structural solution and refinement.

The centrosymmetric space group $C2/m$ (No. 12) was chosen on the basis of the systematic absences (hkl, $h + k \neq 2n$; $h0l$, $h \neq 2n$; $0k0$, $k \neq 2n$) and the statistical analysis of intensity distribution. The structure was solved by Patterson methods (SHELXS-86)[12] and refined on $|F|$ using the full-matrix least-squares technique in MolEN program package.[13] On the basis of 817 reflections and 103 variable parameters, the structure was anisotropically refined to $R = 0.034$, $R_w = 0.037$, and $R_{(zero)} = 0.097$ with the La^{3+} and Ca^{2+} ions statistically disordered on the 4i site, (La(1)/Ca(1): 0.356 74, 0.0, 0.739 67) and (La(2)/Ca(2): 0.071 46, 0.0, 0.745 65). These statistically disordered sites appear to be fully occupied with the occupancies of 0.86 for La(1), 0.14 for Ca(1), 0.82 for La(2), and 0.18 for Ca(2), resulting in an overall stoichiometry of $La_{3.4}Ca_{0.6}V_5Si_4O_{22}$. The final difference electron density map was flat with a maximum of 1.5 e/Å^3 close to V(3) and a minimum of −1.6 e/Å^3 close to La(2)/Ca(2).

Selected X-ray crystallographic data for $La_{3.4}Ca_{0.6}V_5Si_4O_{22}$ are presented in Table 1. The final positional and isotropic thermal parameters of atoms are given in Table 2, selected bond distances are listed in Table 3.

Physical Property Measurements. A SQUID magnetometer (MPMS, Quantum Design) was used for the magnetic susceptibility measurements in the temperature range 4–300 K with an applied field of 1000 G. The room-temperature electrical resistivity was measured with a standard two-probe technique on needle crystals. Ohmic contacts to the crystal were made with a conducting silver paste.

Results and Discussion

Structure. The unit cell structures of $La_{3.4}Ca_{0.6}V_5Si_4O_{22}$ are presented in Figures 1 and 2. As illustrated in Figure 2, $La_{3.4}Ca_{0.6}V_5Si_4O_{22}$ may be formulated more accurately as $La_{3.4}Ca_{0.6}V(Si_2O_7)_2(VO_2)_4$ on the basis of its structural building blocks. The structure of $La_{3.4}Ca_{0.6}V_5Si_4O_{22}$ is built up from layers of vanadium pyrosilicate $V^{III}(Si_2O_7)_2^{9-}$ (the formal oxidation state of the vanadium ions will be discussed later) interconnected with rutile-like layers of $(VO_2)_4^{2.4-}$ by corner-sharing through the oxygen (O(2)) between Si_2O_7 and $V(4)O_6$ polyhedra along the c-axis. The polyhedral network creates distorted octagonal tunnels running along the b-axis, where the La^{3+} and Ca^{2+} ions are statistically disordered. The vanadium pyrosilicate layer is composed of discrete $V(1)O_6$ octahedra and Si_2O_7 groups. Each $V(1)O_6$ octahedron is linked to six Si_2O_7 groups by corner-sharing. The $V(1)O_6$ octahedra and the Si_2O_7 groups are interconnected in the sequence $V(1)O_6-Si_2O_7-V(1)O_6$ along the a- and b-axes. The rutile layer, as shown in Figure 3, consists of two infinite chains of edge-sharing VO_6 octahedra running along the b-axis. One chain is composed of $V(2)O_6$ and $V(3)O_6$ octahedra stacked alternatively along the chain direction, while the other chain is composed of $V(4)O_6$ octahedra only. These two infinite chains of edge-sharing octahedra are linked together by corner-sharing along the a-axis. The angles

Table 2. Atomic Coordinates and $B_{eq}{}^a$ Values for $La_{3.4}Ca_{0.6}V_5Si_4O_{22}$

atom	x	y	z	B_{eq}, Å^2
La(1)/Ca(1)^b	0.35674(6)	0.0	0.73967(7)	0.50(1)
La(2)/Ca(2)^c	0.07146(6)	0.00	0.74565(7)	0.62(1)
V(1)	0.50	0.00	0.50	0.45(5)
V(2)	0.50	0.00	0.00	0.56(5)
V(3)	0.00	0.00	0.00	0.47(5)
V(4)	0.25	0.25	0.00	0.38(3)
Si(1)	0.1393(2)	0.00	0.4566(3)	0.48(5)
Si(2)	0.2961(3)	0.00	0.2679(3)	0.44(5)
O(1)	0.0204(4)	0.248(1)	0.1275(5)	0.6(1)
O(2)	0.2742(4)	0.238(1)	0.1842(5)	0.6(1)
O(3)	0.4091(7)	0.00	0.3392(9)	1.3(2)
O(4)	0.0692(4)	0.236(1)	0.4139(5)	0.9(1)
O(5)	0.1916(7)	0.00	0.5959(8)	0.8(2)
O(6)	0.2149(7)	0.00	0.3583(9)	1.3(2)
O(7)	0.3500(6)	0.00	0.9877(7)	0.4(1)
O(8)	0.1436(7)	0.00	0.9801(7)	0.7(2)

^{a} $B_{eq} = 8\pi^2/3\sum U_{ij}a_ia_ja_i^*a_j$, where the temperature factors are defined as $\exp(-2\pi^2\sum h_ih_ja_i^*a_jU_{ij})$. ^{b} La(1) and Ca(1) have occupancies of 86.0(2)% and 14.0(2)%, respectively. ^{c} La(2) and Ca(2) have occupancies of 82.0(%) and 18.0(2)%, respectively.

Table 3. Selected Interatomic Distances and Angles for $La_{3.4}Ca_{0.6}V_5Si_4O_{22}$

Distances (Å)			
V(1)–O(3)	1.97(1) [2]^a	A(2)–O(1)	2.461(6) [2]
V(1)–O(4)	2.068(7) [4]	A(2)–O(2)	2.541(6) [2]
V(2)–O(1)	1.976(6) [4]	A(2)–O(4)	2.686(7) [2]
V(2)–O(7)	1.996(9) [2]	A(2)–O(5)	2.52(1)
V(3)–O(1)	1.961(7) [4]	A(2)–O(8)	2.599(9)
V(3)–O(8)	1.98(1) [2]	Si(1)–O(4)	1.639(8) [2]
V(4)–O(2)	2.006(6) [2]	Si(1)–O(5)	1.57(1)
V(4)–O(7)	1.961(6) [2]	Si(1)–O(6)	1.62(1)
V(4)–O(8)	1.983(7) [2]	Si(2)–O(2)	1.619(7) [2]
A(1)^b–O(1)	2.446(7) [2]	Si(2)–O(3)	1.58(1)
A(1)–O(2)	2.548(7) [2]	Si(2)–O(6)	1.61(1)
A(1)–O(4)	2.583(7) [2]	Si(1)···Si(2)	3.23(1)^c
A(1)–O(5)	2.484(9)	V(2)–V(3)	2.793(0) [2]
A(1)–O(7)	2.763(9)	V(4)–V(4)	2.793(0) [2]

Angles (deg)			
O(4)–Si(1)–O(4)′	107.2(5)	O(4)–Si(1)–O(5)	114.4(3)
O(4)–Si(1)–O(6)	101.8(3)	O(5)–Si(1)–O(6)	115.8(5)
O(2)–Si(2)–O(2)′	110.8(5)	O(2)–Si(2)–O(3)	110.1(3)
O(2)–Si(2)–O(6)	106.5(3)	O(3)–Si(2)–O(6)	112.9(6)
Si(1)–O(6)–Si(2)	176.3(5)	V(2)–O(7)–V(4)	133.8(3)
V(3)–O(8)–V(4)	133.3(3)		

^{a} [ ] Indicates the number of bonds of this type. ^{b} A represents the statistically disordered La^{3+}/Ca^{2+} ions. ^{c} Nonbonding distance.

(12) Sheldrick, G. M. In *Crystallographic Computing 3*; Sheldrick, G. M., Kruger, C., Goddar, R., Eds.; Oxford University Press: Oxford, U.K., **1985**, pp 175–189.
(13) Fair, C. K. *MolEN*; Enraf-Nonius: 2624 BD Delft, The Netherlands, 1990.

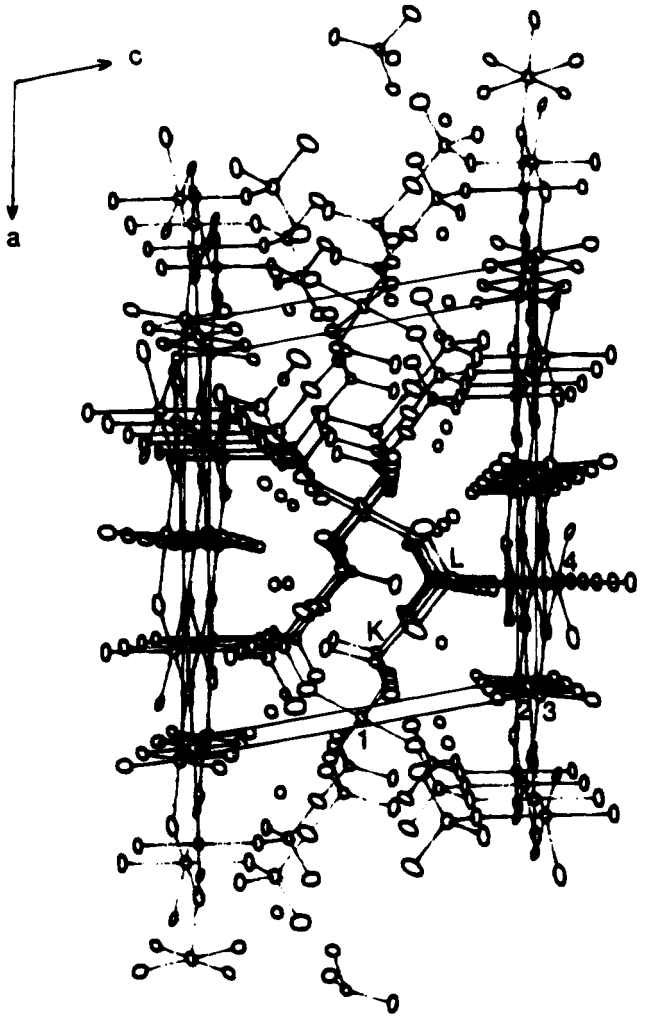

Figure 1. ORTEP drawing (50% thermal ellipsoids) of the unit cell structure of $La_{3.4}Ca_{0.6}V_5Si_4O_{22}$, viewed along the *b*-axis. The numerical labels are for V atoms. Letters K and L represent Si(1) and Si(2), respectively. The non-bonded atoms are the statistically disordered La^{3+}/Ca^{2+} ions.

between two corner-sharing octahedra, V(2)−O(7)−V(4) and V(3)−O(8)−V(4), are 133.8(3) and 133.3(3)°, respectively (Figure 3). Each $V(4)O_6$ octahedron also corner-shares with two Si_2O_7 units along the *c*-axis.

The $Si_2O_7^{6-}$ pyrosilicate unit in $La_{3.4}Ca_{0.6}V(Si_2O_7)_2(VO_2)_4$ corner-shares with five VO_6 octahedra (three isolated $V(1)O_6$ and two edge-sharing $V(4)O_6$) through its five terminal oxygen atoms. The sixth terminal oxygen atom (O(5)) of the $Si_2O_7^{6-}$ unit is bonded with A(1) and A(2) (A represents the statistically disordered La^{3+}/Ca^{2+} ions). A similar $Si_2O_7^{6-}$ group was also observed in $Ba_2(MO)Si_2O_7$ (M = Ti or V),[10,14] where the four terminal oxygen atoms of the pyrosilicate are linked to four MO_5^{6-} square pyramids in the same layer by corner-sharing and two remaining terminal oxygens are associated with Ba^{2+} ions located between $(MO)Si_2O_7^{4-}$ layers. Interestingly, a similar pattern of linkage is rare for the $P_2O_7^{4-}$ group in transition metal pyrophosphates; for example, the $P_2O_7^{4-}$ group in $A_xMP_2O_7$ (A = IA or IIA element) typically shares its six corners with six separate MO_6 octahedra.[15]

All four types of crystallographically independent VO_6 octahedra observed in $La_{3.4}Ca_{0.6}V_5Si_4O_{22}$ are slightly distorted. $V(1)O_6$ is a discrete octahedron with V−O bond distances in the range 1.97(1)−2.068(7) Å (average 2.04 Å). The V−O bond distances fall in the ranges 1.976(6)−1.996(9) Å (average 1.98 Å) for $V(2)O_6$ and 1.961(7)−1.98(1) Å (average 1.97 Å) for $V(3)O_6$. The V−O bond distances of $V(4)O_6$ are in the range 1.961(6)−2.006(6) Å (average 1.98 Å). The average V−O distance of $V(1)O_6$ agrees well with the ionic radius sum (2.02 Å) of VO_6^{9-} calculated from the Shannon effective ionic radii,[16] which strongly suggests that V(1) has a formal oxidation state of 3+. The average V−O distances of $V(2)O_6$, $V(3)O_6$, and $V(4)O_6$, however, do not agree with the ionic radius sum of either VO_6^{9-} or VO_6^{8-}; instead they fall midway between them, suggesting that electrons are, more or less, evenly distributed in the rutile layer of $(VO_2)_4^{2.4-}$. The ionic radius sum calculated from Shannon effective ionic radii is 1.96 Å for VO_6^{8-}.[16] These assessments are consistent with the bond valence sum (BVS)[17] calculations presented in Table 4.

The V−V bonds in the $(VO_2)_4^{2.4-}$ layers of $La_{3.4}Ca_{0.6}V_5Si_4O_{22}$ are extended along the *b*-axis with a uniform distance of 2.793(0) Å between the edge-sharing octahedra, i.e., V(2)−V(3) and V(4)−V(4). A similar extended metal network of V has also been observed in the high-temperature form (T > 340 K) of VO_2 with a regular tetragonal rutile structure and a uniform V−V bond distance of 2.85 Å.[18] The shorter V−V bond distance

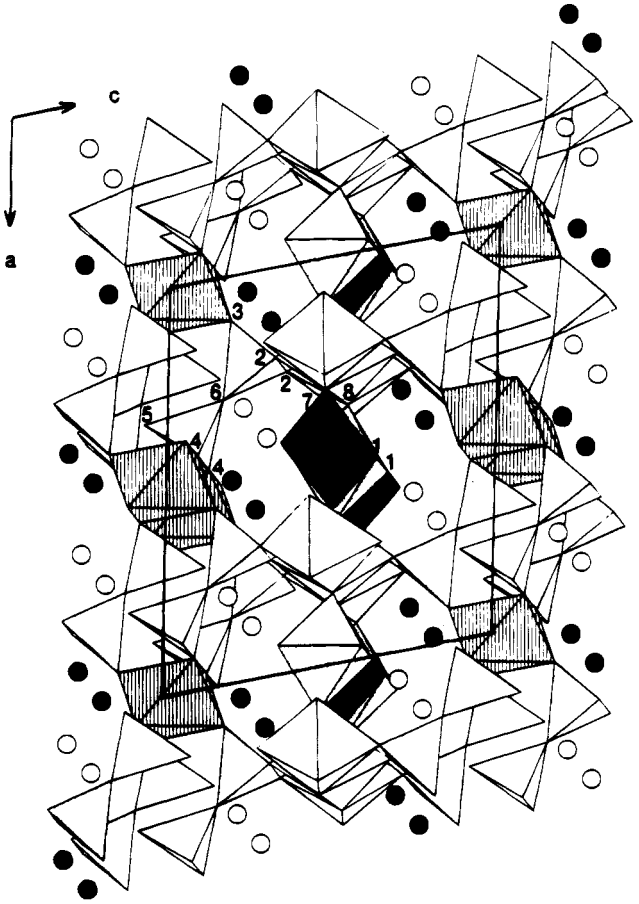

Figure 2. Polyhedral representation of the unit cell structure (shifted by c/2) of $La_{3.4}Ca_{0.6}V_5Si_4O_{22}$, viewed along the *b*-axis. The striped, shaded, dotted, and blank octahedra represent $V(1)O_6$, $V(2)O_6$, $V(3)O_6$ and $V(4)O_6$, respectively. The blank and dotted tetrahedra are the $Si(1)O_4$ and $Si(2)O_4$ in Si_2O_7 units, respectively. The oxygen atoms are numbered. The statistically disordered A(1) and A(2) (A = La^{3+}/Ca^{2+}) ions are represented by the open and solid circles, respectively.

(14) (a) Moore, P. B.; Louisnathan, S. J. *Science.* **1967**, *156*, 1361. (b) Moore, P. B.; Louisnathan, S. J. *Z. Kristallogr.* **1969**, *130*, 438.
(15) Leclaire, A.; Chardon, J.; Borel, M. M.; Raveau, B. *J. Solid State Chem.* **1994**, *109*, 83 and references therein.
(16) Shannon, R. D. *Acta Crystallogr.* **1976**, *A32*, 751.
(17) Brown, I. D.; Altermatt, D. *Acta Crystallogr.* **1985**, *B41*, 244.
(18) Krishna Rao, K. V.; Naidu, S. V.; Ivengar, L. *J. Phys. Soc. Jpn.* **1967**, *23*, 1380.

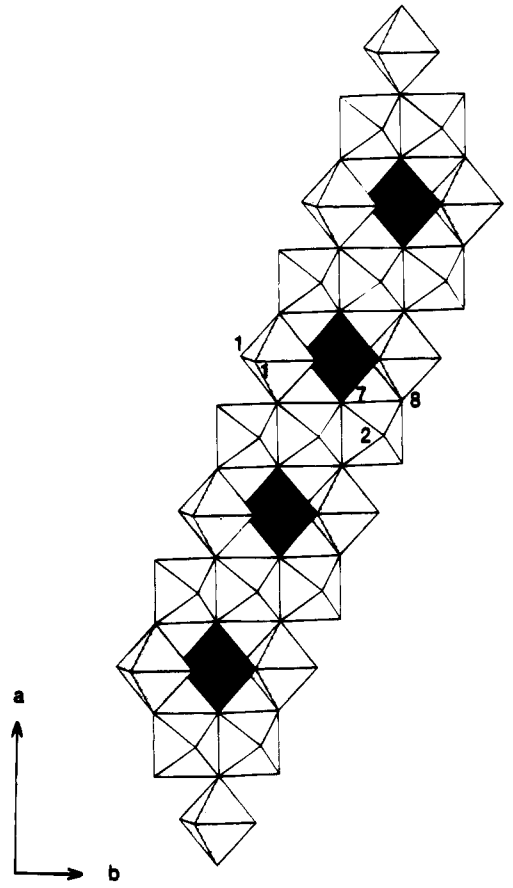

Figure 3. A perspective view of $La_{3.4}Ca_{0.6}V_5Si_4O_{22}$ along the *c*-axis, showing the connectivity of VO_6 octahedra in the $(VO_2)_4^{2.4-}$ rutile layer. The polyhedral representations and the numbering scheme are the same as in Figure 2.

Table 4. Bond Valence Sums (BVS) and Coordination Numbers (CN) for the Crystallographically Independent Atoms in $La_{3.4}Ca_{0.6}V_5Si_4O_{22}$

atom	BVS	CN	atom	BVS	CN
A(1)[a]	2.97[b]	8	O(1)	−2.15	4
A(2)[a]	2.87[b]	8	O(2)	−2.30	4
V(1)	2.75	6	O(3)	−1.78	3
V(2)	3.51	6	O(4)	−1.96	4
V(3)	3.66	6	O(5)	−1.98	4
V(4)	3.51	6	O(6)	−2.13	3
Si(1)	4.09	4	O(7)	−1.90	4
Si(2)	4.19	4	O(8)	−2.08	4

[a] A represents the statistically disordered La^{3+}/Ca^{2+} ions. The occupancies are 86.0(2)% and 14.0(2)% for La(1) and Ca(1), respectively and 82.0(2)% and 18.0(2)% for La(2) and Ca(2), respectively. [b] The BVS assessments for A atoms are based on the La^{3+} ion.

observed in $La_{3.4}Ca_{0.6}V_5Si_4O_{22}$ compared to the high-temperature form VO_2 could be attributed to differences in the number of d electrons per vanadium atom available for metal−metal bonding. Unlike in the high-temperature form of VO_2, which has one d electron for metal−metal bonding, the $(VO_2)_4^{2.4-}$ layers in $La_{3.4}Ca_{0.6}V_5Si_4O_{22}$ have 1.6 electrons per vanadium atom. According to the one-electron energy band diagram proposed for rutile-like structures,[19] the extra electrons in the $(VO_2)_4^{2.4-}$ layers of $La_{3.4}Ca_{0.6}V_5Si_4O_{22}$ populate the V−V σ band with concomitant shortening of the V−V distance. On the other hand, the low-temperature form (T < 340 K) of VO_2 is a distorted rutile structure with monoclinic unit cell, which exhibits alternating long−short V−V bond distances of 3.17 and 2.62 Å.[20]

(19) Rogers, D. B.; Shannon, R. D.; Sleight, A. W.; Gillson, J. L. *Inorg. Chem.* **1969**, *8*, 841.

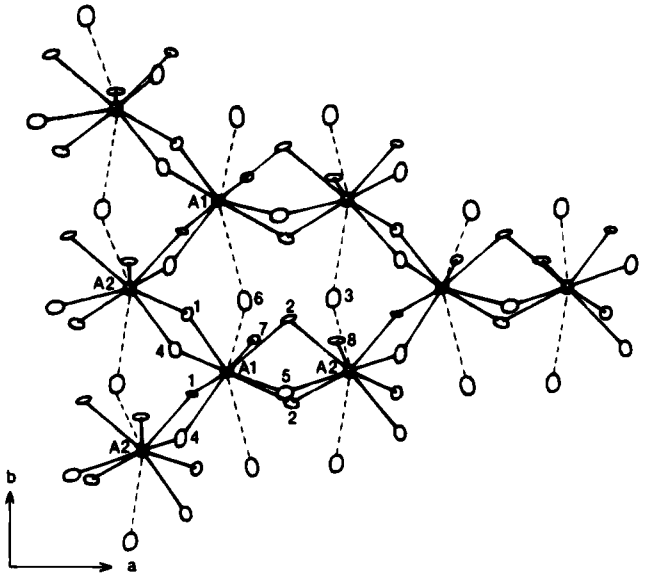

Figure 4. ORTEP drawing (50% thermal ellipsoids) of the coordination environments of A(1) and A(2) in $La_{3.4}Ca_{0.6}V_5Si_4O_{22}$, where A represents the statistically disordered La^{3+}/Ca^{2+} ions. The numerical labels are the same as those in Figure 2.

The Si−O bond lengths are in the ranges 1.57(1)−1.639(8) Å (average 1.617 Å) for $Si(1)O_4$ and 1.58(1)−1.619(7) Å (average 1.607 Å) for $Si(2)O_4$. The O−Si−O angles are between 101.8(3) and 115.8(5)° (average 109.8°) for $Si(1)O_4$ and between 106.5(3) and 112.9(6)° (average 110.1°) for $Si(2)O_4$. The Si(1)−O(6)−Si(2) bridging angle of the pyrosilicate unit is 176.3(5)°. These data are in good agreement with corresponding data reported for silicates[21] and suggest that the SiO_4 tetrahedra are nearly ideal. The bond distances 1.57(1) and 1.58(1) Å for Si(1)−O(5) and Si(2)−O(3), respectively, are relatively short compared to other Si−O distances in the $Si_2O_7^{6-}$ unit. These significantly shorter Si−O distances most likely arise from the electrostatic interactions of the type La^{3+}/Ca^{2+}−O(5)−$Si(1)^{4+}$ and $V(1)^{3+}$−O(3)−$Si(2)^{4+}$, as compared to, for example, that in Si^{4+}−O−Si^{4+} for the central O(6) atom. The low coordination number (CN = 3) of O(3) is also, at least in part, responsible for the short Si(2)−O(3) distance (Table 4). Normally, the $Si-O^b$ (b = bridging) distances are longer than $Si-O^t$ (t = terminal) distances in $Si_2O_7^{6-}$ groups.[3a] The reverse bond order observed for $Si-O^b$ and $Si-O^t$ in $La_{3.4}Ca_{0.6}V_5Si_4O_{22}$ may be attributed to the low coordination number (CN = 3) of the O(6) bridging atoms (Table 4).

As shown in Figure 4, the two statistically disordered ions, A(1) and A(2) (A = La^{3+}/Ca^{2+}), are each eight-coordinated with A−O bond distances ranging from 2.446(7) to 2.763(9) Å (average 2.55 Å) for A(1) and from 2.461(6) to 2.686(7) Å (average 2.56 Å) for A(2). The next long A−O contacts in AO_8 polyhedra are A(1)−O(6), 3.087 (5) Å, and A(2)−O(3), 2.974(4) Å. The A(1) and A(2) polyhedra face-share in neighboring tunnels along the *a*-axis. Each A(1) polyhedron edge-shares with two A(2) polyhedra in the same tunnel along the *b*-axis. A similar pattern of linkages is also observed for the A(2) polyhedron (Figures 2 and 4). Two A(1) and two A(2) polyhedra are each linked along the *b*-axis via weak interactions of A(1)−O(6) and A(2)−O(3), respectively.

Magnetic and Electrical Properties. The temperature-dependent magnetic susceptibility of randomly oriented $La_{3.4}Ca_{0.6}V_5Si_4O_{22}$ crystals (mass ~3.5 mg) is illustrated in Figure 5.

(20) (a) Andersson, G. *Acta Chem. Scand.* **1956**, *10*, 623. (b) Longo, J. M.; Kierkegaard, P. *Acta Chem. Scand.* **1970**, *24*, 420.

(21) Liebau, F. *Structural Chemistry of Silicates: Structure, Bonding, and Classification*; Springer-Verlag: Berlin/New York, 1985; p 16.

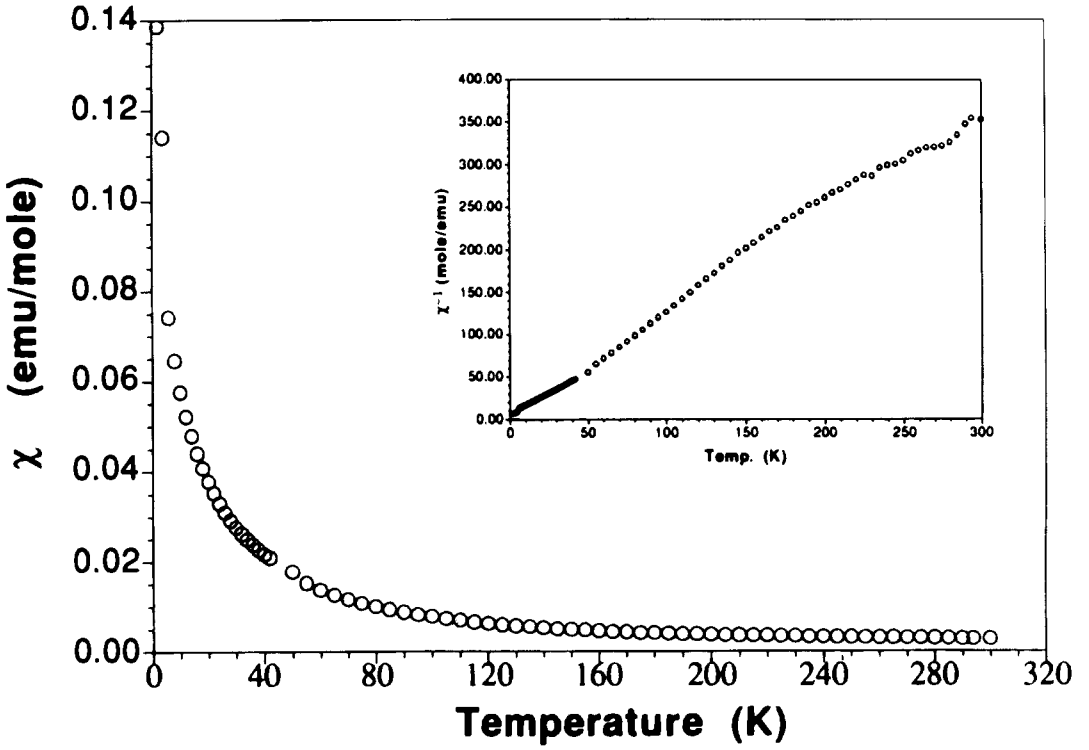

Figure 5. Temperature dependent molar magnetic susceptibility of $La_{3.4}Ca_{0.6}V_5Si_4O_{22}$. The inset shows the variation of inverse susceptibility with temperature.

Variation of the inverse susceptibility as a function of temperature is shown in the inset of Figure 5. The susceptibility values were not corrected for the core diamagnetic contributions of the component ions, because of the large paramagnetic moment of the sample ($\chi_{300K} = 2.83 \times 10^{-3}$ emu/mol). We see no evidence of a long-range magnetic order down to 2 K in $La_{3.4}Ca_{0.6}V_5Si_4O_{22}$. The susceptibility data in the temperature ranges 100−200 and 2−40 K can be fitted to a Curie−Weiss equation:

$$\chi = C/(T - \Theta)$$

where C and Θ are the Curie and Weiss constants, respectively. In the temperature range 100−200 K the Weiss constant, estimated from a least-squares analysis performed on the linear portion of the the χ^{-1} vs T plot, is 7.3 K and the corresponding Curie constant is 0.708 mol K / emu. The effective magnetic moment (μ_{eff}) derived from the Curie constant is 2.4 μ_B. This value of μ_{eff} indicates the presence of nearly two localized electrons per formula unit. The small positive value of the Weiss constant implies weak ferromagnetic correlations between the localized electrons. The Curie and Weiss constants evaluated from the susceptibility data below 40 K are 1.04 mol K/ emu and −7.4 K, respectively. The effective magnetic moment in this temperature range is ~2.8 μ_B, consistent with the presence of two localized electrons. However, the small negative Weiss constant indicates that below 40 K the exchange correlations are weakly antiferromagnetic.

On the basis of the valence count, one would expect 8.4 electrons per formula unit of $La_{3.4}Ca_{0.6}V(Si_2O_7)_2(VO_2)_4$. Of these, two electrons are associated with the isolated $V(1)O_6$ octahedron, in which the formal oxidation state of V, as previously discussed, is 3+. The remaining electrons are presumed to be on the $(VO_2)_4^{2.4-}$ rutile layers. Because of the extended nature of V−O−V interactions in the rutile-like layers, these electrons do not appear to contribute to the total susceptibility, possibly due to (a) electron delocalization in wide conduction bands, (b) formation of metal−metal bonds, or (c) antiferromagnetic correlation in the layers. Thus the observed effective magnetic moment is consistent with the two electrons associated with the $V(1)^{3+}$ ion alone.

The room-temperature electrical resistivities of several needle crystals measured along the needle axis (the *b*-axis) are in the order of 10^6 Ω cm, indicating insulating behavior of $La_{3.4}Ca_{0.6}V_5Si_4O_{22}$. This was somewhat surprising in view of the short V−V distance (2.793 Å) in the $(VO_2)_4^{2.4-}$ layers of $La_{3.4}Ca_{0.6}V_5Si_4O_{22}$ compared to the corresponding distance (2.85Å) in the metallic VO_2 (the high temperature form). The absence of metallic conductivity in $La_{3.4}Ca_{0.6}V_5Si_4O_{22}$ appears to indicate that the electrons in the $(VO_2)_4^{2.4-}$ layer are strongly correlated antiferromagnetically. Neutron diffraction data on oriented single crystals and high-temperature magnetic susceptibility may be able to resolve the ambiguity in the conductivity behavior.

Conclusion

The structure and physical properties of a novel mixed-valent vanadium oxosilicate, $La_{3.4}Ca_{0.6}V_5Si_4O_{22}$, are reported. This compound can be formulated as $La_{3.4}Ca_{0.6}V(Si_2O_7)_2(VO_2)_4$, on the basis of structural building blocks. The $V^{III}(Si_2O_7)_2^{9-}$ and $(VO_2)_4^{2.4-}$ building blocks intergrow along the *c*-axis, and the La^{3+} and Ca^{2+} ions are statistically disordered in distorted octagonal tunnels running along the *b*-axis. The VO_6 octahedron in the $V^{III}(Si_2O_7)_2^{9-}$ building block is isolated by $Si_2O_7^{6-}$ groups. The $(VO_2)_4^{2.4-}$ layer exhibits a regular rutile structure with a uniform V−V bond distance of 2.793 Å. The effective magnetic moment of $La_{3.4}Ca_{0.6}V_5Si_4O_{22}$ can be ascribed to the two unpaired electrons localized in the $V^{III}(Si_2O_7)_2^{9-}$ building block. In view of the extended V−V bond along the *b*-axis, the insulating behavior of $La_{3.4}Ca_{0.6}V_5Si_4O_{22}$ along the *b*-axis was unexpected. The insulating behavior was attributed to antiferromagnetic interactions of electrons in the $(VO_2)_4^{2.4-}$ layers.

Acknowledgment. This work was supported by National Science Foundation Solid State Chemistry Grant DMR-93-14605.

Supplementary Material Available: Tables giving X-ray crystallographic details (Table S1), anisotropic thermal parameters (Table S2), and interatomic distances (Table S3) and angles (Table S4) (7 pages). Ordering information is given on any current masthead page.

IC940727M